minerals

MDPI

Article

In Situ LA-ICP-MS Analysis of Minerals Hosted by Late Cenozoic Basaltic Rocks from Thailand

Long Yuan [1], Quanshu Yan [1,2,3,*], Xuefa Shi [1,2], Haitao Zhang [1,2] and Xijun Liu [4]

1 Key Laboratory of Marine Sedimentology and Environmental Geology, First Institute of Oceanography, Ministry of Natural Resources, Qingdao 266061, China
2 Laboratory for Marine Geology, Qingdao National Laboratory for Marine Science and Technology, Qingdao 266061, China
3 College of Earth Science and Engineering, Shandong University of Science and Technology, Qingdao 266590, China
4 Guangxi Key Laboratory of Hidden Metallic Ore Deposits Exploration, Guilin University of Technology, Guilin 541004, China
* Correspondence: yanquanshu@163.com or qsyan@fio.org.cn

Received: 19 June 2019; Accepted: 17 July 2019; Published: 19 July 2019

Abstract: Shortly after the cessation of seafloor spreading, intraplate magmatism affected large areas in the South China Sea (SCS) region. The origin and geodynamic setting of the post-spreading volcanism is still in debate, for many previous studies have focused on petrogenesis and mantle source of the late Cenozoic basalts from the SCS region. In this study, we obtained in situ major element compositions (by using Electron microprobe analysis—EMPA) and trace element compositions (by using laser ablation inductively coupled plasma mass spectrometry— LA-ICP-MS) for minerals (clinopyroxenes (Cpx), plagioclases (Pl), and olivines (Ol)) hosted by late Cenozoic basaltic rocks from Thailand. The results showed that the olivines had forsterite contents between 60.12% and 84.74%. Clinopyroxene were diopside and augite, and they were enriched in light rare earth elements (LREEs) (La_N/Yb_N = 1.93–4.27) and depleted in large-ion lithophile elements (LILEs). Mineral compositions (mainly based on clinopyroxene) confirmed that these late Cenozoic basaltic rocks were of an intraplate affinity and were similar to contemporaneous basaltic fields in the SCS region (Southern Vietnam, Northern Hainan, and SCS seamounts). Plagioclases were predominantly labradorite, with a few andesine and bytownite, and they were enriched in LREEs and Ba, Sr, and Pb, and most of them exhibited strong positive Eu anomalies. The source lithology of Thailand basaltic rocks could be garnet pyroxenite. The mantle potential temperature beneath Thailand is in the range of 1448–1467 °C, which can be comparable to those beneath Southern Vietnam and Northern Hainan, indicating the Thailand basaltic rocks could be produced by the Hainan mantle plume. In addition, the crystallization temperature of clinopyroxenes (1145–1214 °C) and plagioclase (1067–1133 °C) and their composition characteristics indicate that the magmatic processes have a conspicuous characteristic of fast rate of magma upwelling. Thus, we proposed that the deep geodynamic setting of Thailand late Cenozoic basaltic rocks is similar to those of the whole SCS region, and Hainan mantle plume plays a significant role in the petrogenesis of these basaltic rocks.

Keywords: mineral chemistry; source lithology; magmatic processes; late Cenozoic basalts; Thailand; Hainan plume

1. Introduction

The South China Sea (SCS) region, including Leiqiong Peninsula, the Indochina Block, and the SCS basin itself, lies at the intersection of the Indo–Australian plate, Philippine sea plate (or Pacific

plate), and Eurasian plate (Figure 1). Recent studies have shown that Cenozoic igneous activities in the SCS region are as follows: In the earlier time of Cenozoic (60–43 Ma), bimodal volcanism occurred in the strike-slip rifting basin of the SCS northern continental margin [1–4]. During the Cenozoic seafloor spreading (32–16 Ma) in the SCS, basaltic volcanism occurred in the Pearl River Mouth basin and spreading axis [1]. Shortly after the cessation of seafloor spreading, widespread intraplate volcanism occurred in the SCS region, and the magmatic series of these volcanic activities gradually evolved from tholeiitic to alkalic [5,6]. The post-spreading volcanism has not only affected the SCS basin itself, but also Leiqiong Peninsula and Indochina Peninsula [6–26]. Although many previous studies have focused on petrogenesis and mantle source of the late Cenozoic basalts from the SCS region [6–26], the origin and geodynamic setting of the post-spreading volcanism is still in debate, with present models including: (1) A petrogenetic association with Hainan mantle plume [18,25,26]; (2) origin from the melting of a mixed peridotite/ pyroxenite source [25]; (3) interaction of a mid-ocean ridge basalt (MORB) source with subcontinental lithosphere [8,27]. Understanding the issue of tectonic evolution of the SCS region needs more direct geologic evidence, such as petrologic and geochemical constraints from post-spreading volcanic rocks.

The available geochronological and geochemical data of the SCS region suggest that the younger basalts (8–0.5 Ma) of the SCS seamounts and Indochina block belong to the alkalic series, and the Cenozoic basalts of northern Hainan predominantly belong to the tholeiitic series [10,18,19]. Furthermore, all of the SCS seamounts, Indochina block, and northern Hainan basalts generally display light rare earth element (LREE)-enriched REE patterns and ocean island basalt (OIB)-like trace element compositions [10,18,19,23,25–27]. Isotopic studies on these post-spreading basalts from the SCS region suggested that their mantle source can be explained by a mixing model involving two mantle end members: A moderately depleted Indian MORB-like mantle and an enriched mantle of type 2 (EM2) [6,8,10,13,18,19,22,25–29]. However, although there are a number of studies focusing on whole rock geochemistry for late Cenozoic basaltic rocks from Thailand, in situ major and trace element compositions for these rocks are still lacking, which hinder the ability to understand their petrogenesis and magmatic processes.

In this study, we obtained in situ trace element (by using laser ablation inductively coupled plasma mass spectrometry—LA-ICP-MS) and major element compositions (by using electron microprobe analysis—EMPA) for clinopyroxenes, plagioclases, and olivines in basalts. These data, combined with bulk rock major and trace elements [26], have been used to reveal the source lithology, mantle potential temperature, and primary melt compositions and magmatic processes of late Cenozoic basalts from Thailand. This study provides strong evidence for the Hainan plume affecting post-spreading volcanic activities in Thailand (Indochina block).

2. Geological Setting and Sample Description

Thailand, and its adjacent regions, can be divided into three tectonostratigraphic units: The West Sibumasu Block (Sino–Burma–Malaya–Sumatra), the middle Sukhothai Arc terrane, and the East Indochina Block, which are separated by two sutures [30,31] (Figure 1). One of sutures is the Chiangmai–Chanthaburi Suture, which consists of Middle Devonian to Middle Triassic radiolarian cherts and deep oceanic sediments [26], and the other one is the back-arc Nan-Uttaradit Sra Kaeo Suture, which is composed of a thin block of disaggregated ophiolites and melanges [26,27]. The Sibumasu Block, Indochina Block, and the SCS region were influenced by the Tethys tectonic regime during the late Paleozoic to early Mesozoic, and then by the Pacific Ocean tectonic regime during the late Mesozoic [26,30–32]. During the Cenozoic era (especially for the post SCS spreading period), widespread intraplate volcanism in the SCS also affected Thailand and its adjacent regions (Figure 1). Furthermore, two Cenozoic strike-slip faults (Mae Ping fault and Three Pagodas fault) pass through the Western part of Thailand [26] (Figure 1).

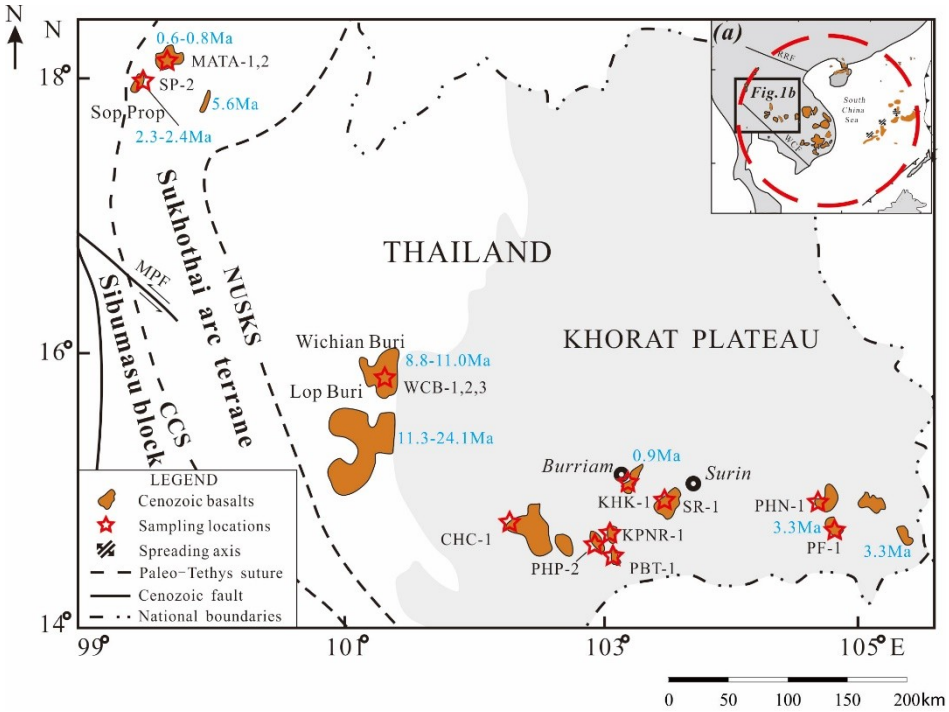

Figure 1. (**a**) Distribution of late Cenozoic intraplate volcanism in the SCS region. The dashed circle (in red) represents the influential cover range of Hainan mantle plume [26]. (**b**) Sketch geological map of Thailand showing Cenozoic fault systems, Cenozoic volcanic centers with age [24,26,27,33], and sampling locations. RRF, Red River fault; WCF, Wang Chao fault; MPF, Mae Ping fault; CCS, Chiangmai-Changthaburi suture; NUSKS, Nan-Uttaradit Sra Kaeo suture.

Late Cenozoic (0.4–11 Ma) basaltic rocks of Thailand are mainly distributed in the Khorat Plateau and the Northern part of the Sukhothai Arc terrane [23,25,26,32]. We collected 14 samples from the 11 basaltic flows of Cenozoic lavas in the Khorat Plateau and the Northern part of the Sukhothai Arc terrane (Figure 1). All basaltic rock samples showed porphyritic textures and contained olivine, clinopyroxene, plagioclase phenocrysts, and some microlites (olivines, clinopyroxenes, and plagioclases) in the groundmass, and these microlites were less than 0.2 mm in size. The phenocryst content was 5–20%, and the olivine content was 30–70% from total phenocrysts. The grain size of olivine phenocrysts mostly varied from 0.4 to 1.2 mm, even to 2 mm (sample SP-2), the shape of which was idiomorphic and hypidiomorphic, and some of which were transformed to iddingsite. The grain size of plagioclase phenocrysts ranged from 0.02×0.20 mm^2–0.20×1.30 mm^2, and most were present as polysynthetic twins. Clinopyroxene phenocrysts were present in some samples (sample CHC-1, PBT-1, PHP-2, PHN-1, and PF-1), the shape of which was idiomorphic and hypidiomorphic. Clinopyroxene phenocrysts had grain sizes of 0.5–1.1 mm, and clinopyroxene phenocrysts of sample CHC-1 had a ring structure.

3. Methods and Results

3.1. Methods

The major elements were analyzed by the JXA-8230 Electron Microprobe Analyzer (EMPA) in Key Laboratory of Marine Sedimentology and Environmental Geology, First Institute of Oceanography, SOA (Qingdao, China). The working conditions of the instrument were as follows: The acceleration voltage was 15 kV, the electron beam current was about 2×10^{-8} A, the electron beam spot was 1 μm, and the quantitative detection limit was about 100 ppm. The standards used in these analyses were albite for Na and Si; orthoclase for K; diopside for Ca; olivine for Mg; haematite for Fe; garnet for Al; chromium oxide for Cr; rutile for Ti; rhodonite for Mn; and nickel silicide for Ni. The analytical

results were corrected by the ZAF method (Z, A, and F represent atomic number, absorption, and fluorescence, respectively). The precision of major element (SiO_2, Al_2O_3, and CaO) analyses was better than 1%, and that of the minor element (Na_2O, K_2O, TiO_2, P_2O_5, MnO, Cr_2O_3, and MgO) analyses was better than 5%. During performing the EMPA analysis, backscattering electron (BSE) images for typical minerals were also obtained (Figure 2). The data were processed with the geochemical software tool "Geokit" [34].

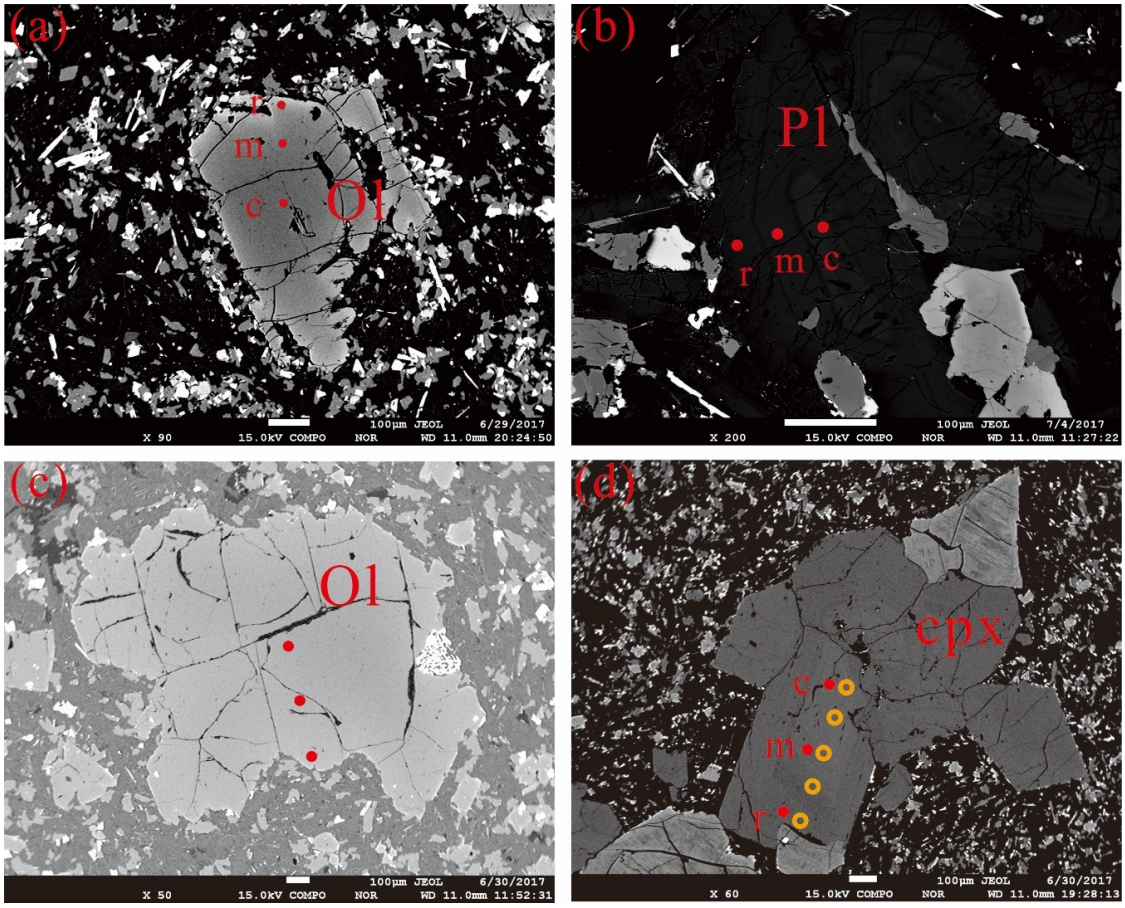

Figure 2. The typical backscattered electron (BSE) images of olivine, clinopyroxene, and plagioclase phenocrysts. (**a**) Olivine phenocryst of sample KHK-1; (**b**) plagioclase phenocryst of sample PF-1; (**c**) olivine phenocryst of sample WCB-1; and (**d**) clinopyroxene phenocryst of sample CHC-1. The yellow circles are the analysis points of sample CHC-1.

In situ analysis of trace elements of minerals hosted by late Cenozoic basaltic rocks from Thailand were conducted at Beijing Createch Testing International Co. Ltd (Beijing, China). Laser sampling was performed using an ESI NWR 193 nm excimer laser ablation system. An Analytik Jena Plasma Quant MS instrument was used to acquire ion-signal intensities. The spot diameter of laser beam was 35 μm and the ablation frequency was 10 Hz. Helium was applied as a carrier gas. Each spot analysis incorporated an approximately 20 s background acquisition from the sample. Element contents were calibrated against multiple reference materials (NIST SRM612 and NIST SRM610). Data calibration using suitable internal standard depended on different samples by Glitter (Si was the internal standard for this experiment). The analysis of most of the elements had an accuracy of less than 5% and a precision greater than 10%.

3.2. Results

3.2.1. Olivine

The analytical results of olivines in late Cenozoic basalic rocks from Thailand are reported in Supplementary Table S1. The olivines had forsterite contents between 60.12% and 84.74%. In the sample of SP-2 from Sukhothai Arc terrane, the Fo content of olivines ranged from 80.87 to 84.60 wt. % (Supplementary Table S1), exhibiting no obvious variations from core to rim of the phenocrysts. In the Khorat Plateau, the Fo contents of olivine phenocrysts and microlites ranged from 60.12% to 84.74% and 66.71% to 73.02%, respectively (Supplementary Table S1). In general, the FeO, MnO, and CaO increased, and NiO decreased, with decreasing Fo content. In some basaltic rock samples (WCB-1, SP-2, and PHN-1), the Fo content of olivine microlites was significantly lower than that of the phenocrysts rim, while that of the other samples was similar to that of the phenocrysts edge. Except for sample MATA-1, some oxides (such as TiO_2, FeO, MnO, and CaO) of olivine phenocrysts in other samples in this study showed no obvious variations from core to rim of the phenocrysts (Supplementary Table S1), suggesting that the chemical compositions of the olivine phenocrysts are relatively uniform.

The CaO contents in olivine ranged from 0.19 to 0.42 wt. %, which is within the range of basaltic phenocrysts (>0.1%) but much higher than mantle peridotite xenoliths (<0.1%) [35]. The grain size of olivines was relatively small and showed no reaction rims, or deformation structures common to olivine xenocrysts, indicating that the olivine phenocrysts of this study were magmatic in origin [36]. In addition, NiO decreased with the decreasing Fo content, which differed from the mantle olivine array [35,37,38] (Figure 3). However, the olivines of one phenocryst from sample WCB-3 (analytical No. WCB-3-4-1 to WCB-3-4-3) had a low CaO content (<0.1%) and relative high Fo content (88.97–90.90), and a large grain size (1.0–1.6 mm), which suggests that they were probably derived from disaggregated xenoliths [39] (Figure 3, Supplementary Table S1).

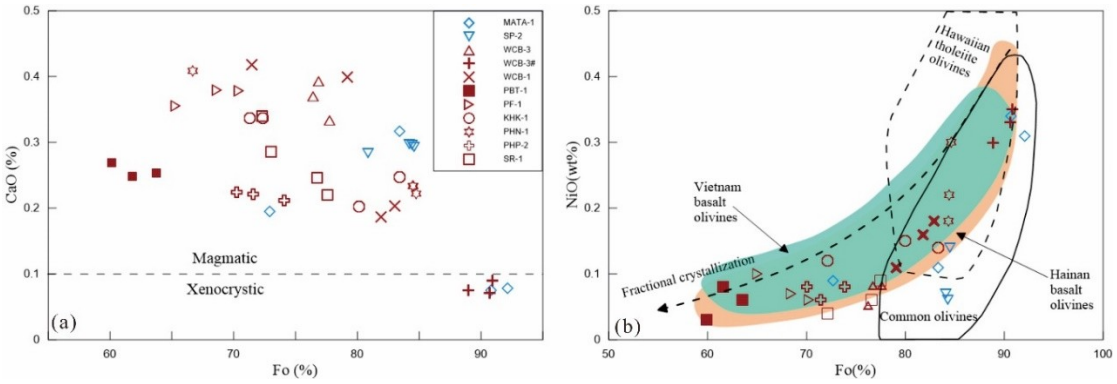

Figure 3. (**a**,**b**) Variations in the composition of olivine phenocrysts. WCB-3# represent the xenocrtstic olivine in sample WCB-3. The dashed line that separates magmatic and xenocrystic olivines on the basis of CaO in (**a**) is from Thompson and Gibson [35]. The field "common olivines" outlines the compositional range of olivines from peridotite xenoliths, orogenic massifs and ophiolites, oceanic abyssal basalt, and mid-ocean ridge basalt (MORB) [37]. In contrast, "Hawaiian tholeiite olivines" denotes the range of olivines from Hawaiian tholeiite basalts [37]. The fractional crystallization is from Sato [38]. "Hainan basalt olivines" is based on Wang et al. [18] and "Vietnam basalt olivines" is based on An et al. [25].

In sample MATA-1, the Fo content of olivine microlite was significantly lower than that of the phenocryst rim. The oxides (such as TiO_2, FeO, MnO, and CaO) of olivine phenocryst in sample MATA-1 showed obvious variations from core to rim of the phenocryst. The olivine of sample MATA-1 had relative high Mg# (core: 90.79–92.15, rim: 83.41), CaO content (core: 0.08, rim: 0.32), and NiO content (core: 0.31–0.34, rim: 0.11), indicating the core of olivine was xenocryst from the mantle rock

and the rim of olivine could simply form over a few years prior to eruption due to magma chamber process (Figure 3).

3.2.2. Clinopyroxene

Major Element Composition

The analytical results of pyroxenes are reported in Supplementary Table S2. Pyroxenes are augite and diopside [40] (Figure 4a). The content of SiO_2 in clinopyroxene changed considerably, ranging from 44.83 to 51.55 wt. %. Some chemical differences between phenocrysts and microlites were identified in this study. For example, in general, the SiO_2 and MgO contents of the clinopyroxene microlites in the groundmass were lower than those of the phenocryst, whereas the TiO_2, FeO, and Na_2O contents of the former were higher than those of the latter, indicating that the evolution of magma enriched Fe and Ti. The Al_2O_3 contents (ranging from 1.43 to 7.03, with an average of 3.90) of clinopyroxene were low in all of the samples, suggesting that these clinopyroxenes were the result of low-pressure crystallization [9].

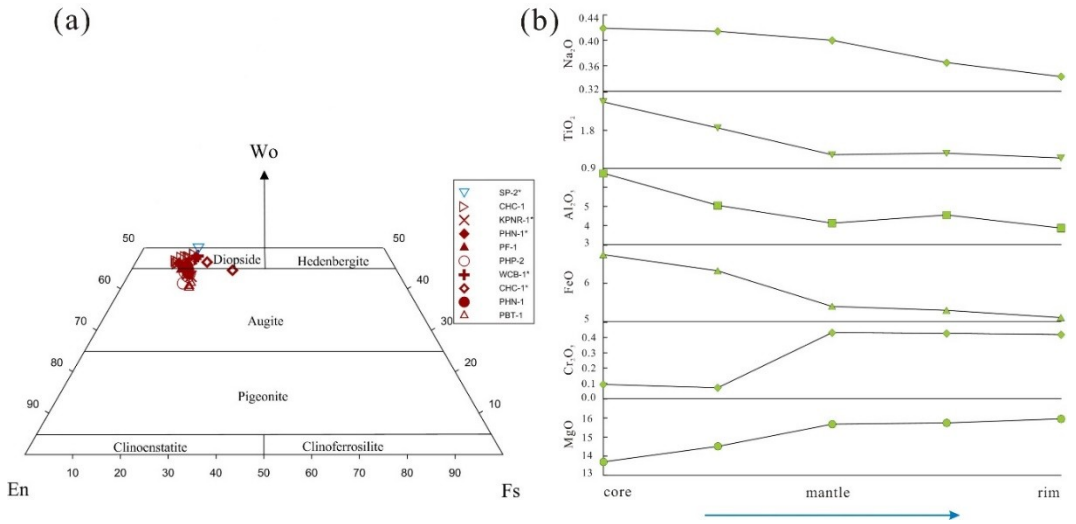

Figure 4. (**a**) Wo-En-Fs diagram of pyroxenes [40], (**b**) The variation in the composition of clinopyroxene with concentric zoning of sample CHC-1. * refers to clinopyroxenes microlites. The five analysis points (yellow circle) are listed in Figure 2c.

Clinopyroxene phenocrysts of sample CHC-1 (analytical No. CHC-1-1 to CHC-1-5) had an obvious concentric zoning. From Supplementary Table S2 and Figure 4b, we can see that MgO and Cr_2O_3 content increased, and FeO, TiO_2, Na_2O, and Al_2O_3 decreased, from core to rim, indicating that the core crystallized in relatively fractionated melts and the rim crystallized in response to introduction of more primitive (Mg and Cr rich) magma into the crystallization environment.

Yan et al. [26] presented the plots of Mg# versus other oxides, CaO/Al_2O_3 and trace elements (Sc, Cr), for basaltic rocks (host rock of these clinopyroxene), and suggested that parent magma derived from mantle source may undergo fractional crystallization of mafic minerals (e.g., olivine and clinopyroxens, etc.) en route to the surface. Figure 5 provides the compositional spectrum of clinopyroxenes. The clinopyroxenes were characterized by low Al_2O_3 contents (inferior to 7.03%). Na_2O, MnO, and TiO_2 did not systematically correlate with Mg#. Cr_2O_3 and Al_2O_3 contents correlated positively with Mg#. FeO contents correlated negatively with Mg#. The inverse FeO-Mg#Cpx trend, though self-correlated because of Mg# = 100 × $Mg^{2+}/(Mg^{2+} + Fe^{2+})$, was purposely plotted to show data coherence [41]. The Cr_2O_3 contents of clinopyroxenes decreased with decreasing Mg#Cpx. Cr was highly compatible in clinopyroxene [41,42]. The decrease of CaO is owing to the fractionation of clinopyroxene, because clinopyroxene fractionation can reduce the CaO content in the residual

melt [18]. The Al_2O_3 and CaO contents decreased with decreasing Mg#Cpx at Mg#Cpx < 80, suggesting that plagioclase fractionation may began at Mg#Cpx = 80, because the crystallization of plagioclase would lower the Al_2O_3 and CaO contents of the melt dramatically [18]. Thus, this study, combined with previous studies [26,43], showed that the order of mineral crystallization of the late Cenozoic basalts of Thailand is as follows, olivine, clinopyroxene, plagioclase.

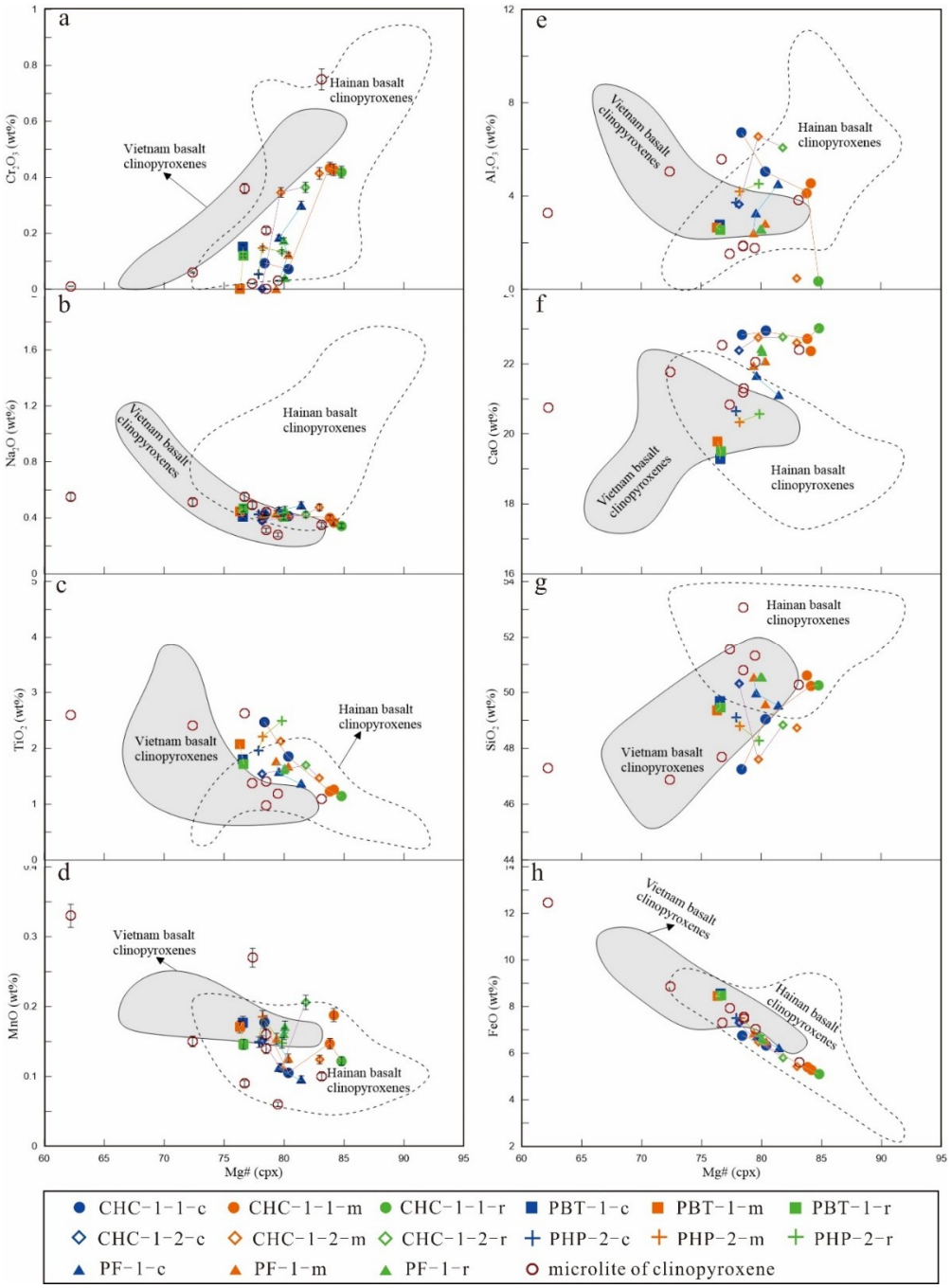

Figure 5. Chemical variations of clinopyroxenes phenocrysts. Data for northern Hainan basalts are from Wang et al. [18], and data for Vietnam are from Hoang et al. [43]. c-core; m-mantle; r-rim. The analyses of core–mantle–rim in a single phenocryst is linked by broken line. (**a**) Cr_2O_3 vs. Mg#; (**b**) Na_2O vs. Mg#; (**c**) TiO_2 vs. Mg#; (**d**) MnO vs. Mg#; (**e**) Al_2O_3 vs. Mg#; (**f**) CaO vs. Mg#; (**g**) SiO_2 vs. Mg#; (**h**) FeO vs. Mg#.

Trace Element Composition

Trace element concentrations of clinopyroxenes from late Cenozoic basalts from Thailand are listed in Supplementary Table S3. The total concentrations of rare earth elements (ΣREE) of clinopyroxenes ranged from 52 to 214 ppm, with an average of 84 ppm, which was slightly higher than that of clinopyroxenes from the contemporaneous lavas of other areas in the South China Sea region (with an average of 62 ppm) [6]. Except for one phenocryst from sample WCB-3 (analytical no. WCB-3-4-1 to WCB-3-4-6) (Supplementary Table S3), compared to clinopyroxenes from other areas in the SCS region [9,14], other clinopyroxenes (both phenocrysts and microlites) exhibited light rare earth element enrichment (LREE), with relatively high ratio of LREE/HREE (ranging from 2.51 to 4.73, with an average value of 3.28), La_N/Yb_N (ranging from 1.93 to 4.27, with an average value of 2.89), Ce_N/Yb_N (ranging from 2.43 to 5.04, with an average value of 3.88), and Sm_N/Yb_N (ranging from 2.81 to 7.38, with an average value of 5.27) (Figure 6, Supplementary Table S3). Furthermore, these clinopyroxenes had a relatively low ratio of La_N/Nd_N (ranging from 0.44–0.88, with an average value of 0.58) and La_N/Sm_N (ranging from 0.39–1.22, with an average value of 0.61). These clinopyroxenes from the sample of PHN-1 and PF-1 showed slightly negative Eu anomalies (Eu/Eu* = 0.81–0.88, with an average of 0.85) and no obvious Ce anomalies (Figure 6, Supplementary Table S3), indicating slight fractionation of plagioclase during the magma process. Note that one clinopyroxene phenocryst from sample WCB-3 (analytical no. WCB-3-4-1 to WCB-3-4-6) showed a relative flatted chondrite-normalized REE pattern (Figure 5a) and no obvious Eu and Ce anomalies, with constant ratio of LREE/HREE (ranging from 2.27 to 2.36, with an average value of 2.32) and La_N/Yb_N (ranging from 1.20 to 1.34, with an average value of 1.25), indicating the clinopyroxenes of WCB-3 may be not phenocrysts, but xenocrysts, which is consistent with the occurrence of olivine xenocrysts in the same sample, suggesting that mantle xenocrysts are entrained by sample WCB-3 during its ascent to the surface.

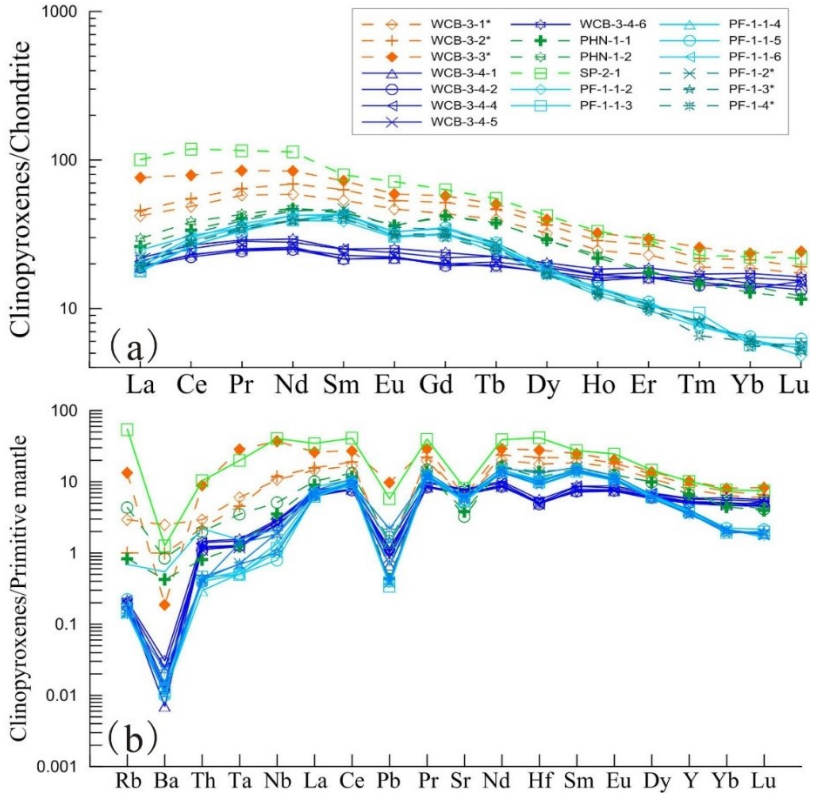

Figure 6. (**a**) Chondrite-normalized rare earth element (REE) patterns for the clinopyroxenes from the late Cenozoic basaltic rocks of Thailand, (**b**) primitive mantle-normalized trace element diagram for clinopyroxenes from the late Cenozoic basaltic rocks of Thailand. Data for chondrite and primitive mantle are from Sun and McDonough [44]. * refers to clinopyroxenes microlites.

In primitive mantle-normalized trace element spider diagrams (Figure 6b), most samples were generally depleted in large-ion lithophile elements (LILEs) (such as Ba and Sr), indicating the fractionation of plagioclase during the magma process, because the Ba and Sr were mainly entered into K-rich and Ca-rich minerals in the form of isomorphism.

3.2.3. Plagioclase

Major Element Composition

The analytical results of plagioclases are reported in Supplementary Table S4. The plagioclase in this study were predominantly labradorite, with a few andesine and bytownite (Figure 7). The An value of plagioclase microlites from the Sukhothai Arc terrane ranged from 58.84 to 63.76 (Supplementary Table S4). In contrast, the An value of plagioclase phenocrysts from the Khorat Plateau ranged from 44.48 to 70.71, and the An value of plagioclase microlites in these lavas ranged from 40.27 to 60.56 (Supplementary Table S4). In addition, plagioclase phenocrysts in sample PHN-1 basalt had a typical concentric zoning, possibly representing the rapid cooling stage when magma erupts. In general, the high An value of the plagioclase in this study indicate that the plagioclase was formed in a rapidly upwelling magma environment [10].

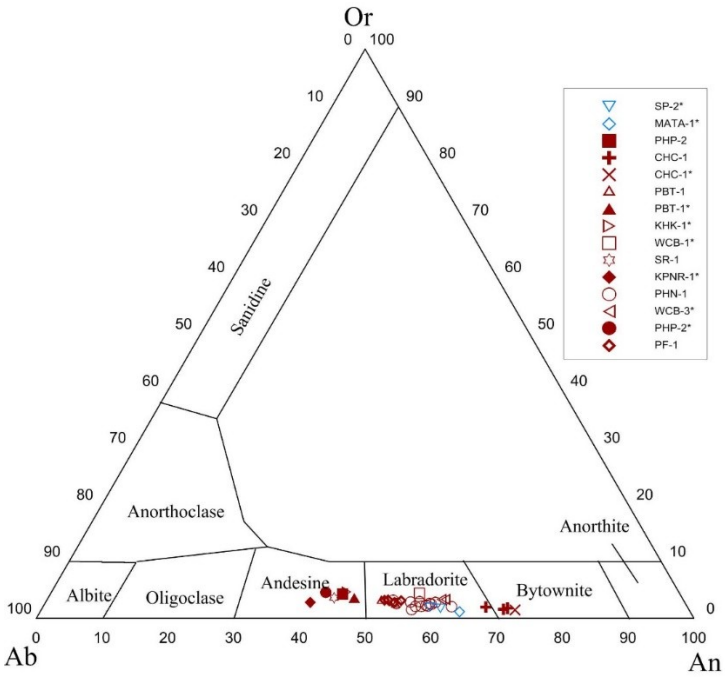

Figure 7. Classification of plagioclase in terms of its composition. * refers to plagioclases microlites.

Trace Element Composition

Trace element concentrations of plagioclases are reported in Supplementary Table S5. In primitive mantle-normalized trace element spider diagrams and chondrite- normalized REE patterns (Figure 8a,b), all of the plagioclases were enriched in LREEs. Except for MATA-1, most of the plagioclase samples exhibited strong positive Eu anomalies (Figure 8a) and enrichment of Ba, Sr, and Pb (Figure 8b). However, the plagioclases of MATA-1 showed negative Eu anomalies and depletion of Ba and Sr. The plagioclase with negative Eu anomalies can form during the late stage of granitic magma [45], indicating the clinopyroxenes of MATA-1 may be not phenocrysts, but xenocrysts, which could have been trapped by sample MATA-1 during its ascent to the surface.

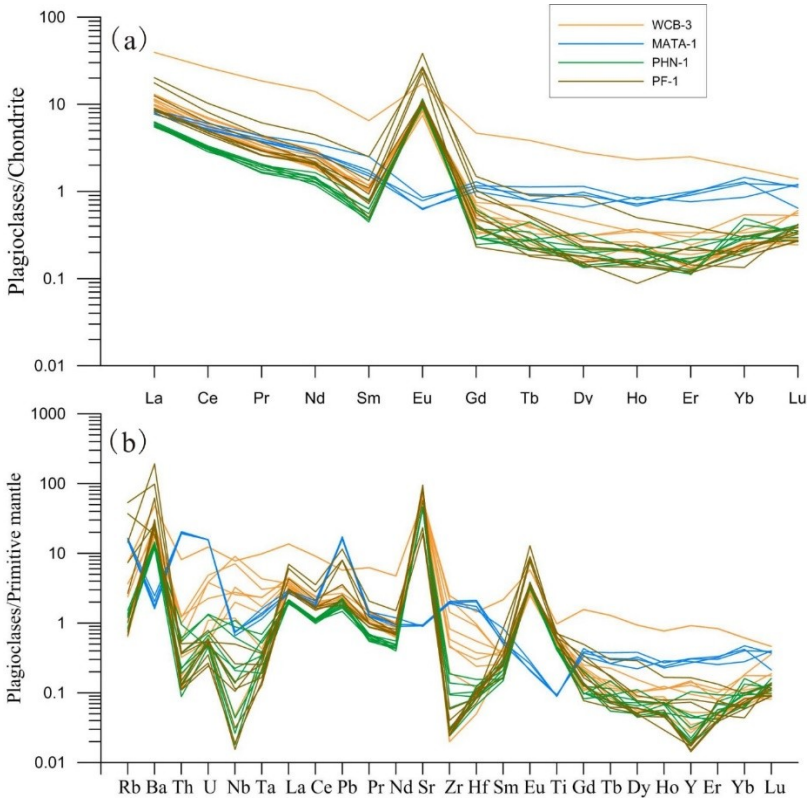

Figure 8. (**a**) Chondrite-normalized REE patterns for the plagioclases from the late Cenozoic basaltic rocks of Thailand, (**b**) Primitive mantle-normalized trace element spider diagram for plagioclases from the late Cenozoic basaltic rocks of Thailand. Data for chondrite and primitive mantle are from Sun and McDonough [44].

4. Discussion

4.1. Nature of the Source Lithology

Traditional radiogenic isotopic studies (e.g., Sr-Nd-Pb-Hf) have shown that the mantle source of late Cenozoic basalt from the Indochina Block can be explained by a binary mixing model, one is a Indian MORB-like mantle, and the other is EM2, which may have originated from Hainan plume [6,22,25–27,29]. Previous authors have investigated the geochemical characteristics and petrogenesis of these basaltic rocks in past decades [23–27]. However, there is still in debate on the nature of the source lithology. Previous studies have proposed different rock types as pre-melting mantle source rocks, e.g., garnet pyroxenite, garnet peridotite, and recycled upper oceanic crust-derived eclogite/pyroxenite [18,25,26,43,46,47]. In recent decades, researchers have successfully used the Fe/Mn ratio, FC3MS parameter ($FeO_T/CaO - 3 \times MgO/SiO_2$), CaO content, Dy/Yb ratio, and Yb content to indicate the nature of the source lithology [18,25,26,43,46–48]. Based on these experimental parameters [43,46,47], we used the whole-rock major element compositions [26] to deduce the nature of the source lithology of the Thailand late Cenozoic basaltic rocks (Table 1). The results are as follows. (1) These basaltic rocks had high Fe/Mn ratios (>60) that fall within the pyroxenite-derived melt field (Figure 9a), which is similar to the case for contemporaneous basaltic rocks from Southern Vietnam [25,43]. (2) The majority of these basaltic rocks had high FC3MS values (>0.5), which are plotted within the pyroxenite-derived melt field in the FC3MS-MgO diagram (Figure 9b), which is consistent with those contemporaneous basaltic rocks from Southern Vietnam and Hawaiian basalts [37,43]. (3) These basaltic rocks had low CaO contents, which are plotted within the pyroxenite-derived melt field in the CaO-MgO diagram (Figure 9c), which is similar to contemporaneous basaltic rocks from Southern Vietnam [43], and the olivine phenocrysts inherited this low-CaO signature. According to the above

results, we assessed the presence of pyroxenite in the mantle source of Thailand basalts. The basaltic rocks of this study had high Dy/Yb ratio and relatively low Yb content [26], indicating that the basalts were derived from a garnet-bearing mantle source. In addition, the effective melting pressure and melting temperature based on the primary melts were P_f = 22.3–27.4 kbar and T = 1425–1442 °C (Table 1), which is in accordance with the transition of source lithology from spinel to garnet lherzolite [49]. This suggests that the basaltic rocks in this study were derived from a garnet-bearing mantle source.

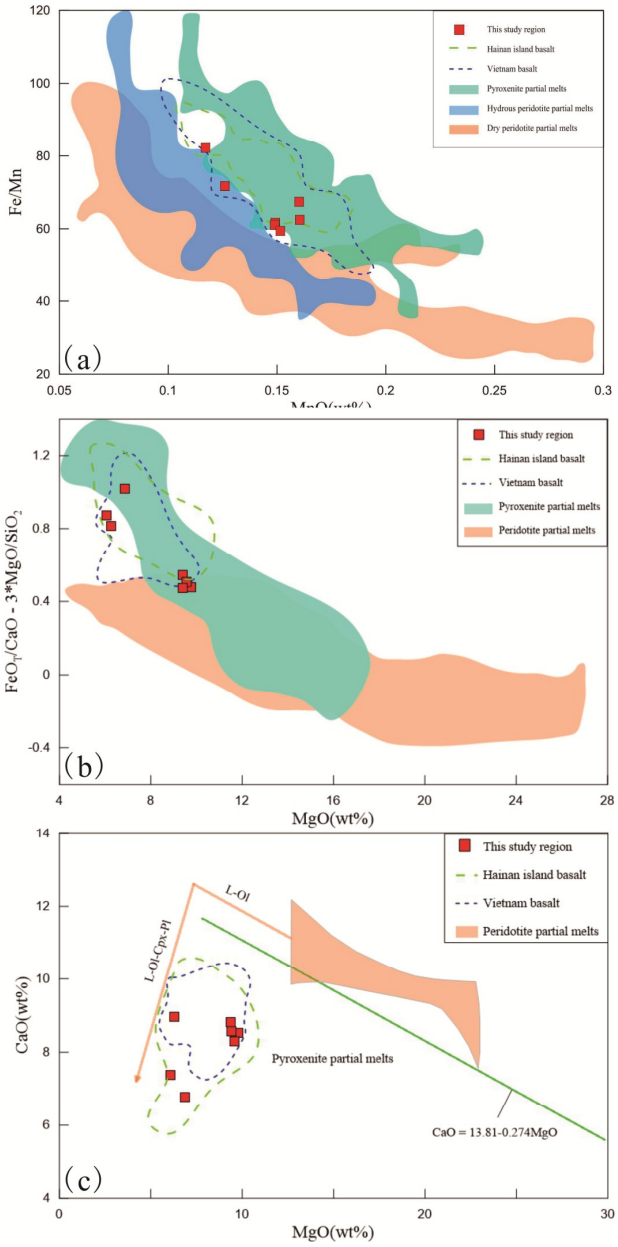

Figure 9. (**a**) MnO vs. Fe/Mn, (**b**) MgO vs. $FeO_T/CaO - 3 \times MgO/SiO_2$, (**c**) MgO vs. CaO values for Thailand late Cenozoic basaltic rocks (MgO content > 6 wt. %). The fields showing experimental melts in (**a**) are modified from Liu et al. [46]. Data for Northern Hainan basalts are from Wang et al. [18], and data for Vietnam are from Hoang et al. [43]. The fields showing experimental melts in (**b**) are modified from Liu et al. [46]. Data for Vietnam are from Hoang et al. [43]. The thick green line in (**c**) separates peridotite- and pyroxenite-sourced primary melts [48]. The dashed orange arrow in (**c**) indicates the typical liquid line of descent (LLD) for primary magmas that crystallize gabbro in the crust [48]. Data for this study region are from Yan et al. [26].

Bulk rock trace element concentrations of host rocks can also provide some invaluable information on the source lithology. Experimental petrology shows that the concentration of a trace element in melt C_L is related to its concentration in the source mantle C_0 by the expression. $C_L/C_0 = 1/[F + D_{RS}(1 - F)]$, where F is the degree of melting and D_{RS} is the bulk distribution coefficient of the residual solids [50,51]. Here, we assumed that the source is similar to the primitive mantle as defined by Sun and McDonough [43]. Thus, La_N, Sm_N, Yb_N represent C_L/C_0 of La, Sm, Yb, respectively. The expression can be changed into $(La/Sm)_N = [F + D_{Sm}(1\text{-}F)]/ [F + D_{La}(1 - F)]$ and $(La/Yb)_N = [F + D_{Yb}(1 - F)]/ [F + D_{La}(1 - F)]$ [50,51]. Where D_{La}, D_{Sm}, D_{Yb} are bulk distribution coefficients of the residual solids of La, Sm, Yb. Trace element mineral/melt partition coefficients are from Kelemen et al. [52]. The calculated results are shown in Supplementary Table S6. The $(La/Yb)/_N$ in basaltic rocks of this study range from 9.05 to 25.35 [26], indicating the basalts were derived from a garnet-bearing mantle source. The $(La/Sm)/_N$ in basaltic rocks of this study range from 1.85 to 3.79, suggesting the basalts may have been produced by the degree of melting ranging from 5%–20% of garnet pyroxenite, which is similar to the results of Vietnam and Hainan [18,25]. Thus, bulk rock major- and trace element compositions give a consistent result for the source lithology of late Cenozoic basaltic rocks from Thailand, garnet pyroxenite.

4.2. Primary Melt Compositions and the Mantle Potential Temperature

Primary melt compositions have been widely used to estimate the thermal state of mantle sources [25,53–58]. The major element data of the late Cenozoic basalts from Thailand have been provided in Yan et al. [26]. The correlation of MgO and CaO contents suggests that the effect of clinopyroxene fractionation in the Thailand basalts likely took place at MgO contents <8 wt. %. Therefore, to minimize the influence of clinopyroxene fractionation, only samples with MgO contents >8 wt. % were chosen as the starting composition. The primary melt compositions for the Thailand basalts were estimated (Table 1) by adding small (0.1%) increments of olivine ($Fo = 90.1$) to samples with MgO contents <8 wt. %, supposing the olivine-melt distribution coefficient $K_D\ (Fe/Mg)^{Ol/liq} = 0.31$, $Fe^{2+}/(Fe^{2+} + Fe^{3+}) = 0.9$ in the melt (Roder and Emslie, 1970). Melting conditions and mantle potential temperatures (T_p; Table 1) were estimated based on primary melt compositions [18,25,55–61].

The effective melting pressure (P_f) and melting temperature (T) based on the primary melts were $P_f = 22.3$–27.4 kbar (average value = 23.9 kbar) and $T = 1425$–1442 °C (average value = 1430 °C), which are similar to ranges characteristic of Southern Vietnam ($P_f = 29.6$–32.8 kbar, $T = 1470$–1480 °C) and Northern Hainan basalts ($P_f = 18$–32 kbar, $T = 1420$–1530 °C) (Table 1) [18,25]. The mantle potential temperature beneath Thailand varies from 1448 to 1467 °C, which is slightly lower than Southern Vietnam (1468–1490 °C) and north of Hainan Island (1500–1580 °C) (Table 1), indicating that the mantle source of Thailand basaltic rocks, similar to those of Southern Vietnam and Northern Hainan, is related to the Hainan mantle plume [18,25]. The slightly lower T_p of late Cenozoic basaltic rocks from Thailand than those from northern Hainan Island and southern Vietnam may reflect that some energy is consumed when the mantle plume material flows along the lithosphere rheology boundary layer westward to farther Thailand region (relative to Vietnam and Hainan). Specifically, the T_p of northern Hainan Island, near the center of mantle plume, was higher than that of the Indochina Peninsula, which is more distant from the center of the mantle plume.

Table 1. Estimated primary melt compositions, mantle potential temperatures and melting conditions for representative samples of late Cenozoic basaltic rocks from Thailand. H_2O content in primary melt was estimated by fractionation correction of Ce. F (degree of melting) was estimated by Equation (A2) of Putirka et al. [56]. P_{f1} to P_{f3} are effective melting pressures in kbar. P_{f1} is defined by Haase [54]; P_{f2} is defined by Albarede [53]; P_{f3} is the average of P_{f1} to P_{f2}. T_1 to T_3 are the melting temperatures (°C) of the melt segregation. T_1 is according to Herzberg et al. [57]; T_2 is according to Putirka [59]; T_3 is the average of T_1 to T_2. T_{P1} to T_{P4} are the mantle potential temperature in °C. T_{P1} was estimated using the MgO contents in the primary melts following Herzberg et al. [57]; T_{P2} was estimated following Herzberg et al. [60]; T_{P3} was estimated following Putirka [61]; T_{P4} is the average of T_{P1} to T_{P3}.SD, standard deviation. Data for Northern Hainan basalts are from Wang et al. [18], and data for Vietnam are from An et al. [25].

Starting Sample	WCB-1	WCB-2	WCB-3	MATA-2	Southern Vietnam	Northern Hainan
Rock type	Trachybasalt	Trachybasalt	Trachybasalt	Basanite	Basanite	
Olivine add (%)	15	15	17	16	13–15	18–25
SiO_2	47.3	47.1	47.3	45.9		
TiO_2	1.7	1.7	1.7	1.9		
Al_2O_3	13.2	13.8	13.3	12.9		
Cr_2O_3	0.0	0.0	0.0	0.0		
Fe_2O_3	0.8	0.9	0.8	1.0		
FeO	8.8	8.7	8.6	9.5		
MnO	0.2	0.2	0.2	0.2	-	
MgO	15.3	15.2	15.9	15.1		
CaO	7.5	7.3	7.4	7.7		
Na_2O	2.8	2.9	2.5	3.2		
K_2O	1.9	2.0	1.9	2.2		
NiO	0.0	0.0	0.0	0.0		
P_2O_5	0.4	0.4	0.4	0.4		
H_2O	1.0	1.0	1.0	1.6		
F (%)	13.0	12.4	15.5	7.1	4–7	14–19
P_{f1}	24.8	25.9	25.0	30.9	33.6–36.6	17.2–33.7
P_{f2}	19.8	20.5	20.7	23.9	27.5–30.4	15.6–30.2
P_{f3}	22.3	23.2	22.9	27.4	29.7–32.8	17.8–31.6
SD	2.5	2.7	2.1	3.5	3–4	1.5–3.6
T_1	1457	1457	1471	1464	-	-
T_2	1396	1394	1412	1391	1444–1459	1429–1514
T_3	1426	1425	1442	1427	1463–1480	1420–1529
SD	30	31	30	36	16–22	3–34
T_{P1}	1466	1464	1481	1461	-	-
T_{P2}	1442	1440	1458	1437	1469–1482	1454–1536
T_{P3}	1447	1443	1462	1445	1458–1496	1413–1611
T_{P4}	1452	1449	1467	1448	1468–1490	1468–1561
SD	10	11	10	10	1–9	25–55

4.3. Physical Conditions of Crystallization

4.3.1. Crystallization Pressure and Temperature of Clinopyroxenes

In recent decades, many researchers have proposed various thermobarometers for calculating crystallization pressures and temperatures of clinopyroxene formation [59,62–64]. Putirka et al. [62] established a series of thermodynamic equations based on experimental work that relates temperature and pressure to equilibrium constants and allows for the construction of clinopyroxene-liquid thermobarometers. However, the thermobarometers were only applied to the basaltic magma temperature and pressure calculation, with an application range of 1110–1475 °C and 0.4–0.9 GPa. Putirka et al. [59] experimentally re-calibrated the thermobarometers and established a new equilibrium temperature and pressure formula that can be applied to mafic magma and intermediate-acid magma. In this study we used the Putirka [59] equation to calculate the crystallization pressures and temperatures of clinopyroxenes (Table 2) [59]. The calculated results showed that temperature and pressure ranges were 1145–1214 °C (average value = 1190 °C) and 0.4–0.9 GPa (average value = 0.7 GPa), respectively, which is similar to the SCS basin (1095–1261 °C, 0.4–1.5 GPa) and Northern Hainan Island (1100–1250 °C, 0.7–1.5 GPa) (Table 2) [9,18]. Based on the calculated pressures, the depth of magma chambers of late

Cenozoic basaltic rocks (including basanite, basalt, trachybasalt, and basaltic trachyandesite) calculated from equilibrium temperatures and pressures between clinopyroxene and melt can be inferred to 11 to 26 km, which is in the middle and upper part of the continental crust.

4.3.2. Crystallization Pressure and Temperature of Plagioclase

Kudo and Weill [65] proposed the first plagioclase-liquid geothermometer. Subsequently, many workers proposed various thermobarometers for calculating crystallization pressures and temperatures of plagioclase formation. In this study, we used the methods from Kudo and Weill and Putirka [59,65] to calculate the crystallization pressures and temperatures of plagioclase (Table 2). It was found that the crystallization temperature based on the Kudo and Weill [65] geothermometer was similar to the temperature determined based on the Putirka [59] thermobarometer. However, since the geothermometer of Kudo and Weill [62] does not consider whether the melt and plagioclase reached equilibrium and the effect of water on the plagioclase crystallization, we adopted the pressure and temperature calculations based on Putirka [59].

Table 2. Crystallization temperatures and pressures of the clinopyroxenes and plagioclases in late Cenozoic basaltic rocks from Thailand and surrounding regions. The crystallization temperature and pressure of the clinopyroxenes and plagioclases were estimated following Putirka [59].

Regions	Clinopyroxene		Plagioclase		References
	T (°C)	*P* (Gpa)	*T* (°C)	*P* (Gpa)	
Thailand	1145–1214	0.4–0.9	1067–1133	0.3–0.9	This study
Hainan Island	1100–1250	0.7–1.5	-	-	Wang et al. [18]
South China Sea basin	1095–1261	0.4–1.5	927–1179	-	Yan et al. [9,10]
Okinawa trough	-	-	1012–1280	-	Chen et al. [66]

The crystallization pressures and temperatures of plagioclase from the Thailand basalts were 0.3–0.9 GPa (average value = 0.6 GPa) and 1067–1133 °C (average value = 1095 °C) (Table 2), which can be comparable to those for the SCS regions (927–1179 °C), and the Okinawa trough (1012–1280 °C) (Table 2) [10,66].

4.4. Tectonic Implications

The tectonic setting for late Cenozoic basaltic rocks in the Indochina block is still not clear, and they may be related to plate tectonics processes [22,23], or to the mantle plume [25,26]. Major- and trace element compositions of clinopyroxene can provide some information for tectonic setting of host rock. Base on clinopyroxene compositions [67–69], Aparicio [67] developed Na-Fe-Mn triangular diagram to distinguish the tectonic setting of the host rock, and Nisbet and Pearce [70] developed TiO_2-Na_2O-MnO triangular diagram to determine the tectonic setting of the host rock. In Figure 10a, all samples are plotted in the within-plate volcanism field, indicating that these basaltic rocks in this study were formed in an intraplate tectonic setting. In addition, there were obvious distinctions between the clinopyroxene samples with high Mg# and low Mg#, and this may have been caused by fractionation or the contamination process. In the TiO_2-Na_2O-MnO triangular diagram, all clinopyroxenes are also plotted in the field of WPA (Figure 10b), suggesting that the host rock of these clinopyroxenes could be within-plate basalts. In addition, the clinopyroxenes in this study belong to Ca-Mg-Fe series, which are beneficial to the isomorphism of REE, owing to REE existing mainly in the form of isomorphism in clinopyroxene [71]. We used the clinopyroxene/melt partition coefficient [49] and REE contents (measured in this study) of clinopyroxenes in late Cenozoic basaltic rocks in Thailand to calculate the hypothetical parental melt (shown on Figure 11), which were similar to the host rock of the clinopyroxenes [26] (Figure 11), with typical feature of intraplate OIB [52].

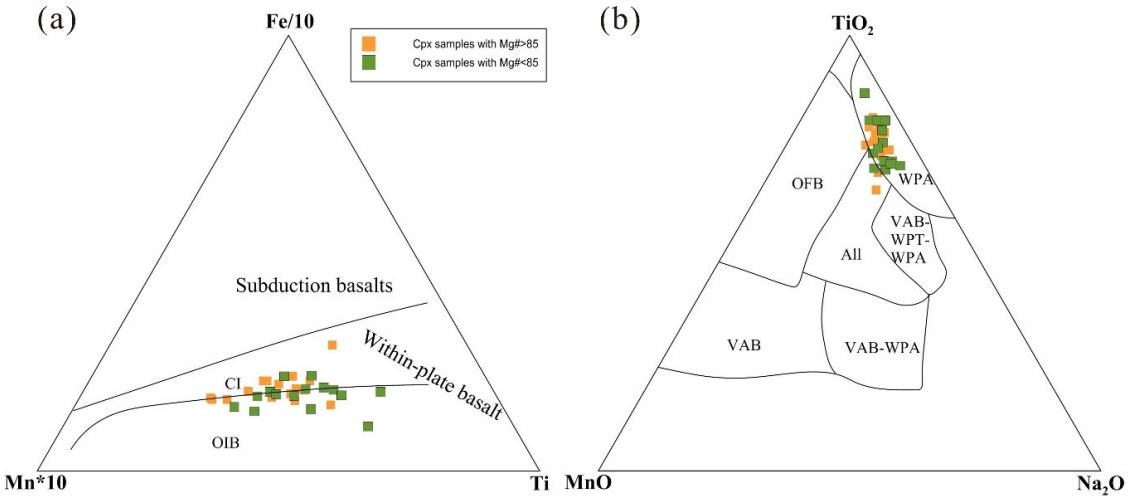

Figure 10. Tectonic discrimination diagrams of Fe/10-Ti-Mn × 10 (**a**) and TiO_2-MnO-Na_2O tectonic discrimination diagram (**b**) for clinopyroxenes. The curve is based on Aparicio [67]. CI: alkaline volcanism thinned continental crust; OIB: oceanic island basalt. The TiO_2-MnO-Na_2O tectonic discrimination diagram is developed by Nisbet and Pearce [70]. WPT: within-plate tholeiitic basalt; WPA: within-plate alkali basalt; VAB: volcanic arc basalt; OFB: ocean floor basalt.

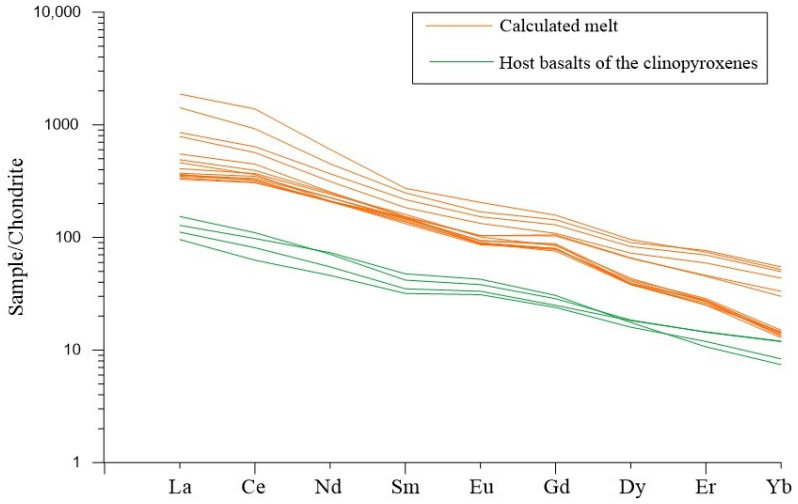

Figure 11. Calculated chondrite-normalized REE patterns of the parental magma of the clinopyroxenes (based on clinopyroxene compositions). Data for host basalts are from Yan et al. [26].

Recent geophysical and geochemical studies have shown that there is a mantle plume beneath Hainan Island [6,9,72,73]. Seismic tomographic studies have also shown that there is a sub-vertical low-velocity column, extending from shallow depths to the 660 km discontinuity, and even reaching 1300 km depth beneath Hainan Island and the SCS [72,74,75]. Due to the existence of the Hainan mantle plume, the alkaline volcanic rocks of the Indochina Peninsula and the SCS exhibit OIB-like characteristics, with high potential mantle temperature [6,18,25]. In this study, the volcanic rocks were composed of basanite, basalt, trachybasalt, and basaltic trachyandesite, and trace element patterns of these rocks showed typical OIB-like characteristics [26]. These, together with high T_p and the nature of the source lithology (garnet pyroxenite), indicate that the mantle beneath Thailand has been affected by the mantle plume.

5. Conclusions

(1) The order of mineral crystallization of the late Cenozoic basalts of Thailand was olivine, clinopyroxene, plagioclase, which is consistent with that of typical OIB. The source lithology of the Thailand basaltic rocks could be garnet pyroxenite.

(2) The clinopyroxene discrimination diagrams exhibited that the parental-magma formed in an intraplate tectonic setting environment.

(3) The crystallization pressure and temperature of clinopyroxenes in late Cenozoic basaltic rocks in Thailand ranged from 0.4–0.9 GPa and 1145–1214 °C, similar to those of the SCS basin and northern Hainan Island. The crystallization pressure and temperatures of plagioclase ranged from 0.3–0.9 Gpa and 1067 °C to 1133 °C, which is similar to those for the SCS. The above characteristics showed that parental magmas of late Cenozoic basaltic rocks from Thailand had experienced multiphase crystallization and fractionation during its ascent to the surface. Moreover, the plagioclase had a high An content, suggesting that it was produced during the rapid upwelling of magma.

(4) The effective melting pressure and melting temperature based on the primary melts were 22.3–27.4 kbar and 1425–1442 °C, respectively, which was similar to the northern Hainan Island and the Southern Vietnam. The mantle potential temperature beneath Thailand is in the range 1448–1467 °C, slightly lower than north of Hainan Island and Southern Vietnam.

(5) This study provides some additional important evidence (e.g., magmatic processes, mantle potential temperatures) for the Hainan mantle plume affecting Thailand and other areas in the Indochina block (e.g., Vietnam).

Supplementary Materials: The following are available online at http://www.mdpi.com/2075-163X/9/7/446/s1, Table S1 Electron probe analyses (wt. %) of olivines in basalt from the Thailand. Table S2 Electron probe analyses (wt. %) of clinopyroxene in basalt from the Thailand. Table S3 LA-ICP-MS analysis (ppm) of clinopyroxene in basalt from the Thailand. Table S4 Electron probe analyses (wt. %) of plagioclase in basalt from the Thailand. Table S5 LA-ICP-MS analysis (ppm) of plagioclase in basalt from the Thailand. Table S6 Estimated (La/Sm)N and (La/Yb)N through partial melting of primitive mantle.

Author Contributions: L.Y., Q.Y., and X.S. conceived the experiments; L.Y., Q.Y., H.Z., and X.L., conducted experiments; L.Y., Q.Y., and X.S., wrote the manuscript. All authors analyzed data, contributed to interpretive aspects and reviewed the manuscript.

Funding: This research was funded by the National Programme on Global Change and Air-Sea Interaction (No. GASI-GEOGE-02), Basic Scientific Fund for National Public Research Institutes of China (2016S01), the Scientific and Technological Innovation Project Financially Supported by Qingdao National Laboratory for Marine Science and Technology (No. 2016ASKJ05), the National Natural Science Foundations of China (grants Nos. 41776070, U1606401, 41230960, 41322036), AoShan Talents Program Supported by Qingdao National Laboratory for Marine Science and Technology (No. 2015ASTP-ES16) and Taishan Scholarship from Shandong Province.

Acknowledgments: We thank Igor Ashchepkov and two anonymous reviewers for their constructive comments and suggestions. We thank LetPub (www.letpub.com) for its linguistic assistance during the preparation of this manuscript.

Conflicts of Interest: The authors declare no conflict of interest.

References

1. Zou, H.P.; Li, P.L.; Rao, C.T. Geochemistry of Cenozoic volcanic rocks in Zhujiangkou basin and its geodynamic significance. *Geochimica* **1995**, *24*, 33–45.
2. Chung, S.-L.; Cheng, H.; Jahn, B.-M.; O'Reilly, S.Y.; Zhu, B. Major and trace element, and Sr-Nd isotope constraints on the origin of Paleogene volcanism in South China prior to the South China Sea opening. *Lithos* **1997**, *40*, 203–220. [CrossRef]
3. Li, P.L.; Liang, H.X.; Dai, Y.D.; Liu, H.M. Origin and tectonic setting of the Yanshanian igneous rocks in the Pearl River Mouth basin. *Guangdong Geol.* **1999**, *14*, 1–8.

4. Zhou, H.; Xiao, L.; Dong, Y.; Wang, C.; Wang, F.; Ni, P. Geochemical and geochronological study of the Sanshui basin bimodal volcanic rock suite, China: Implications for basin dynamics in southeastern China. *J. Asian Earth Sci.* **2009**, *34*, 178–189. [CrossRef]
5. Li, S.T.; Lin, C.S.; Zhang, Q.M. Dynamic process of episodic rifting in continental marginal basin and tectonic events since 10 Ma in South China Sea. *Chin. Sci. Bull.* **1998**, *43*, 797–810.
6. Yan, Q.; Shi, X.; Castillo, P.R. The late Mesozoic–Cenozoic tectonic evolution of the South China Sea: A petrologic perspective. *J. Asian Earth Sci.* **2014**, *85*, 178–201. [CrossRef]
7. Kudrass, H.; Wiedicke, M.; Cepek, P.; Kreuzer, H.; Muller, P. Mesozoic and Cainozoic rocks dredged from the South China Sea (Reed Bank area) and Sulu Sea and their significance for plate-tectonic reconstructions. *Mar. Pet. Geol.* **1986**, *3*, 19–30. [CrossRef]
8. Tu, K.; Flower, M.; Carlson, R.W.; Xie, G.H.; Chen, C.Y.; Zhang, M. Magmatism in the South China basin. *Chem. Geol.* **1992**, *97*, 47–63. [CrossRef]
9. Yan, Q.S.; Shi, X.F.; Wang, K.S.; Bu, W.R. Mineral chemistry and its genetic significance of olivine in Cenozoic basalts from the South China Sea. *Acta Pet. Sin.* **2007**, *23*, 2981–2989.
10. Yan, Q.S.; Shi, X.F.; Liu, J.; Chang, L.H.; Yin, J. Chemical composition of plagioclase in Cenozoic alkali basalt from the South China Sea. *Acta Miner. Sin.* **2008**, *28*, 135–142.
11. Yan, Q.S.; Shi, X.F.; Yang, Y.; Wang, K.S. Potassium-argon/argon-40-argon-39 geochronology of Cenozoic alkali basalts from the South China Sea. *Acta Oceanol. Sin.* **2008**, *27*, 115–123.
12. Yan, Q.S.; Shi, X.F.; Wang, K.S.; Bu, W.R.; Xiao, L. Major element, trace element, and Sr, Nd and Pb isotope studies of Cenozoic basalts from the South China Sea. *Sci. China Ser. D-Earth Sci.* **2008**, *51*, 550–566. [CrossRef]
13. Yan, Q.; Castillo, P.; Shi, X.; Wang, L.; Liao, L.; Ren, J. Geochemistry and petrogenesis of volcanic rocks from Daimao Seamount (South China Sea) and their tectonic implications. *Lithos* **2015**, *218*, 117–126. [CrossRef]
14. Zhang, Y.; Yu, K.; Qian, H. LA-ICP-MS Analysis of Clinopyroxenes in Basaltic Pyroclastic Rocks from the Xisha Islands, Northwestern South China Sea. *Minerals* **2018**, *8*, 575. [CrossRef]
15. Zhou, B.; Wang, H.F.; Mao, C.; Zhu, N.; Huang, R.; Peng, J. Geochronology of and Nd-Sr-Pb isotopic evidence for mantle source in the ancient subduction zone beneath Sanshui Basin, Guangdong Province, China. *Acta Geochem.* **1989**, *8*, 65–71.
16. Jia, D.C.; Qiu, X.L.; Hu, R.Z.; Lu, Y. Geochemical nature of mantle reservoirs and tectonic setting of basalts in Beibu Gulf and its adjacent region. *Trop. Oceanol.* **2003**, *22*, 30–39.
17. Li, C.N.; Wang, F.Z.; Zhong, C.S. Geochemistry of quaternary basaltic volcanic rocks of weizhou island in Beihai city of Guangxi and a discussion on characteristics of their source. *Acta Pet. Miner.* **2005**, *24*, 28–34.
18. Wang, X.C.; Li, Z.X.; Li, X.H.; Li, J.; Liu, Y.; Long, W.G.; Zhou, J.B.; Wang, F. Temperature, pressure, and composition of the mantle source region of late Cenozoic basalts in Hainan Island, SE Asia: A consequence of a young thermal mantle plume close to subduction zones? *J. Pet.* **2012**, *53*, 177–233. [CrossRef]
19. Zou, H.; Fan, Q. U–Th isotopes in Hainan basalts: Implications for sub-asthenospheric origin of EM2 mantle endmember and the dynamics of melting beneath Hainan Island. *Lithos* **2010**, *116*, 145–152. [CrossRef]
20. Barr, S.M.; Macdonald, A.S. Geochemistry and geochronology of late Cenozoic basalts of Southeast Asia: Summary. *Geol. Soc. Am. Bull.* **1981**, *92*, 1069–1142. [CrossRef]
21. Barr, S.; Dostal, J. Petrochemistry and origin of megacrysts in Upper Cenozoic basalts, Thailand. *J. Asian Earth Sci.* **1986**, *1*, 107–116. [CrossRef]
22. Hoang, N.; Flower, M.F.; Carlson, R.W. Major, trace element, and isotopic compositions of Vietnamese basalts: Interaction of hydrous EM1-rich asthenosphere with thinned Eurasian lithosphere. *Geochim. Cosmochim. Acta* **1996**, *60*, 4329–4351. [CrossRef]
23. Hoang, N.; Flower, M. Petrogenesis of Cenozoic Basalts from Vietnam: Implication for Origins of a 'Diffuse Igneous Province'. *J. Pet.* **1998**, *39*, 369–395. [CrossRef]
24. Barr, S.; Cooper, M. Late Cenozoic basalt and gabbro in the subsurface in the Phetchabun Basin, Thailand: Implications for the Southeast Asian Volcanic Province. *J. Asian Earth Sci.* **2013**, *76*, 169–184. [CrossRef]
25. An, A.-R.; Choi, S.H.; Yu, Y.; Lee, D.-C. Petrogenesis of Late Cenozoic basaltic rocks from southern Vietnam. *Lithos* **2017**, *272*, 192–204. [CrossRef]
26. Yan, Q.; Shi, X.; Metcalfe, I.; Liu, S.; Xu, T.; Kornkanitnan, N.; Sirichaiseth, T.; Yuan, L.; Zhang, Y.; Zhang, H. Hainan mantle plume produced late Cenozoic basaltic rocks in Thailand, Southeast Asia. *Sci. Rep.* **2018**, *8*, 2640. [CrossRef]

27. Zhou, P.; Mukasa, S.B. Nd Sr Pb isotopic, and major- and trace-element geochemistry of Cenozoic lavas from the Khorat Plateau, Thailand: Sources and petrogenesis. *Chem. Geol.* **1997**, *137*, 175–193. [CrossRef]
28. Yan, Q.; Straub, S.; Shi, X. Hafnium isotopic constraints on late Miocene to Pliocene seamount basalts from the South China Sea and its tectonic implications. *J. Asian Earth Sci.* **2019**, *171*, 162–168. [CrossRef]
29. Choi, S.H.; Mukasa, S.B.; Kwon, S.T.; Andronikov, A.V. Sr, Nd, Pb and Hf isotopic compositions of late Cenozoic alkali basalts in south Korea: Evidence for mixing between the two dominant asthenospheric mantle domains beneath east Asia. *Chem. Geol.* **2006**, *232*, 134–151. [CrossRef]
30. Metcalfe, I. Palaeozoic–Mesozoic history of SE Asia. *Geol. Soc. Lond. Spéc. Publ.* **2011**, *355*, 7–35. [CrossRef]
31. Metcalfe, I. Gondwana dispersion and Asian accretion: Tectonic and palaeogeographic evolution of eastern Tethys. *J. Asian Earth Sci.* **2013**, *66*, 1–33. [CrossRef]
32. Yan, Q.; Metcalfe, I.; Shi, X. U-Pb isotope geochronology and geochemistry of granites from Hainan Island (northern South China Sea margin): Constraints on late Paleozoic-Mesozoic tectonic evolution. *Gondwana Res.* **2017**, *49*, 333–349. [CrossRef]
33. McCabe, R.; Celaya, M.; Cole, J.; Han, H.-C.; Ohnstad, T.; Paijitprapapon, V.; Thitipawarn, V. Extension tectonics: The Neogene opening of the north–south trending basins of central Thailand. *J. Geophys. Res. Solid Earth* **1988**, *93*, 11899–11910. [CrossRef]
34. Lu, Y.F. Geokit-A geochemical toolkit for Microsoft Excel. *Geochimica* **2004**, *33*, 459–464, (In Chinese with English Abstract).
35. Thompson, R.N.; Gibson, S.A.; Thompson, R.N.R.N.; Gibson, S.S.A. Transient high temperatures in mantle plume heads inferred from magnesian olivines in Phanerozoic picrites. *Nature* **2000**, *407*, 502–506. [CrossRef]
36. Xu, Y.; Huang, X.; Menzies, M.A.; Wang, R. Highly magnesian olivines and green-core clinopyroxenes in ultrapotassic lavas from western Yunnan, China: Evidence for a complex hybrid origin. *Eur. J. Miner.* **2003**, *15*, 965–975. [CrossRef]
37. Sobolev, A.V.; Hofmann, A.W.; Sobolev, S.V.; Nikogosian, I.K. An olivine-free mantle source of Hawaiian shield basalts. *Nature* **2005**, *434*, 590–597. [CrossRef]
38. Sato, H. Nickel content of basaltic magmas: Identification of primary magmas and a measure of the degree of olivine fractionation. *Lithos* **1977**, *10*, 113–120. [CrossRef]
39. Larsen, L.M.; Pedersen, A.K. Processes in High-Mg, High-T Magmas: Evidence from Olivine, Chromite and Glass in Palaeogene Picrites from West Greenland. *J. Pet.* **2000**, *41*, 1071–1098. [CrossRef]
40. Morimoto, N. Nomenclature of pyroxenes. *Miner. Pet.* **1988**, *39*, 55–76. [CrossRef]
41. Stone, S.; Niu, Y. Origin of compositional trends in clinopyroxene of oceanic gabbros and gabbroic rocks: A case study using data from ODP Hole 735B. *J. Volcanol. Geotherm. Res.* **2009**, *184*, 313–322. [CrossRef]
42. Hart, S.R.; Dunn, T. Experimental cpx/melt partitioning of 24 trace elements. *Contrib. Miner. Pet.* **1993**, *113*, 1–8. [CrossRef]
43. Hoang, T.H.A.; Choi, S.H.; Yu, Y.; Pham, T.H.; Nguyen, K.H.; Ryu, J.-S. Geochemical constraints on the spatial distribution of recycled oceanic crust in the mantle source of late Cenozoic basalts, Vietnam. *Lithos* **2018**, *296*, 382–395. [CrossRef]
44. Sun, S.-S.; Mc Donough, W. Chemical and isotopic systematics of oceanic basalts: Implications for mantle composition and processes. *Geol. Soc. Lond. Spéc. Publ.* **1989**, *42*, 313–345. [CrossRef]
45. Wang, J.M.; Ding, G.C. The negative Eu Anomaly of Feldspar in Suzhou A-type Granite and its origin significance. *Dizhi Shiyanshi* **1995**, *11*, 108–111, (In Chinese with English Abstract).
46. Liu, Y.; Gao, S.; Kelemen, P.B.; Xu, W. Recycled crust controls contrasting source compositions of Mesozoic and Cenozoic basalts in the North China Craton. *Geochim. Cosmochim. Acta* **2008**, *72*, 2349–2376. [CrossRef]
47. Yang, Z.-F.; Zhou, J.-H. Can we identify source lithology of basalt? *Sci. Rep.* **2013**, *3*, 1856. [CrossRef]
48. Herzberg, C.; Asimow, P.D. Petrology of some oceanic island basalts: PRIMELT2.XLS software for primary magma calculation. *Geochem. Geophys. Geosyst.* **2008**, *9*. [CrossRef]
49. Klemme, S.; O'Neill, H.S. The near-solidus transition from garnet lherzolite to spinel lherzolite. *Contrib. Miner. Pet.* **2000**, *138*, 237–248. [CrossRef]
50. Shaw, D.M. Trace element fractionation during anataxis. *Geochim. Cosmochim. Acta* **1977**, *34*, 237–243. [CrossRef]
51. Tamura, Y.; Ishizuka, O.; Sato, T.; Nichols, A.R.L. Nishinoshima volcano in the Ogasawara Arc: New continent from the ocean? *Isl. Arc* **2018**, *28*, e12285. [CrossRef]

52. Kelemen, P.B.; Shimizu, N.; Dunn, T. Relative depletion of niobium in some arc magmas and the continental crust: Partitioning of K, Nb, La and Ce during melt/rock reaction in the upper mantle. *Earth Planet. Sci. Lett.* **1993**, *120*, 111–134. [CrossRef]
53. Albarède, F. How deep do common basaltic magmas form and differentiate? *J. Geophys. Res. Solid Earth* **1992**, *97*, 10997–11009. [CrossRef]
54. Haase, K.M. The relationship between the age of the lithosphere and the composition of oceanic magmas: Constraints on partial melting, mantle sources and the thermal structure of the plates. *Earth Planet. Sci. Lett.* **1996**, *144*, 75–92. [CrossRef]
55. Kelley, K.A.; Terry, P.; Grove, T.L.; Stolper, E.M.; Sally, N.; Erik, H. Mantle melting as a function of water content beneath back-arc basins. *J. Geophys. Res. Solid Earth* **2006**, *111*. [CrossRef]
56. Putirka, K.D.; Perfit, M.; Ryerson, F.; Jackson, M.G. Ambient and excess mantle temperatures, olivine thermometry, and active vs. passive upwelling. *Chem. Geol.* **2007**, *241*, 177–206. [CrossRef]
57. Herzberg, C.; Gazel, E. Petrological evidence for secular cooling in mantle plumes. *Nature* **2009**, *458*, 619–622. [CrossRef]
58. Shellnutt, J.G.; Pham, T.T. Mantle Potential Temperature Estimates and Primary Melt Compositions of the Low-Ti Emeishan Flood Basalt. *Front. Earth Sci.* **2018**, *6*, 67. [CrossRef]
59. Putirka, K.D. Thermometers and Barometers for Volcanic Systems. *Rev. Miner. Geochem.* **2008**, *69*, 61–120. [CrossRef]
60. Herzberg, C.; Asimow, P.D.; Arndt, N.; Niu, Y.; Lesher, C.M.; Fitton, J.G.; Cheadle, M.J.; Saunders, A.D. Temperatures in ambient mantle and plumes: Constraints from basalts, picrites, and komatiites. *Geochem. Geophys. Geosyst.* **2007**, *8*. [CrossRef]
61. Putirka, K.D. Mantle potential temperatures at Hawaii, Iceland, and the mid-ocean ridge system, as inferred from olivine phenocrysts: Evidence for thermally driven mantle plumes. *Geochem. Geophys. Geosyst.* **2005**, *6*. [CrossRef]
62. Putirka, K.; Johnson, M.; Kinzler, R.; Longhi, J.; Walker, D. Thermobarometry of mafic igneous rocks based on clinopyroxene-liquid equilibria, 0-30 kbar. *Contrib. Miner. Pet.* **1996**, *123*, 92–108. [CrossRef]
63. Ashchepkov, I.; André, L.; Downes, H.; Belyatsky, B.; Ashchepkov, I. Pyroxenites and megacrysts from Vitim picrite-basalts (Russia): Polybaric fractionation of rising melts in the mantle? *J. Asian Earth Sci.* **2011**, *42*, 14–37. [CrossRef]
64. Ashchepkov, I.; Ntaflos, T.; Logvinova, A.; Spetsius, Z.; Downes, H.; Vladykin, N.; Ashchepkov, I. Monomineral universal clinopyroxene and garnet barometers for peridotitic, eclogitic and basaltic systems. *Geosci. Front.* **2017**, *8*, 775–795. [CrossRef]
65. Kudo, A.M.; Weill, D.F. An igneous plagioclase thermometer. *Miner. Pet.* **1970**, *25*, 52–65. [CrossRef]
66. Chen, X.M.; Tan, Q.Q.; Zhao, G.T. Plagioclases from the basalt of Okinawa trough and its petrogenesis significance. *Acta Miner. Sin.* **2002**, *18*, 482–488.
67. Aparicio, A. Relationship between clinopyroxene composition and the formation environment of volcanic host rocks. *IUP J. Earth Sci.* **2010**, *4*, 1–11.
68. Gilman, T.; Feineman, M.; Fisher, D. The Chulitna terrane of south-central Alaska: A rifted volcanic arc caught between the Wrangellia composite terrane and the Mesozoic margin of North America. *Geol. Soc. Am. Bull.* **2009**, *121*, 979–991. [CrossRef]
69. Tang, D.; Qin, K.; Chen, B.; Mao, Y.; Guo, H.; Evans, N.J. Mineral chemistry and genesis of the Permian Cihai and Cinan magnetite deposits, Beishan, NW China. *Ore Geol. Rev.* **2017**, *86*, 79–99. [CrossRef]
70. Nisbet, E.G.; Pearce, J.A. Clinopyroxene composition in mafic lavas from different tectonic settings. *Contrib. Miner. Pet.* **1977**, *63*, 149–160. [CrossRef]
71. Lai, S.C.; Qin, J.F.; Li, Y.F. Trace element geochemistry and classification of the Clinopyroxene in Cenozoic trachybasalt from north Qiangtang area, Tibetan Plateau. *J. Northwest Univ.* **2005**, *25*, 611–616.
72. Lebedev, S.; Nolet, G. Upper mantle beneath southeast Asia from S velocity tomography. *J. Geophys. Res. Solid Earth* **2003**, *108*. [CrossRef]
73. Lei, J.; Zhao, D.; Steinberger, B.; Wu, B.; Shen, F.; Li, Z. New seismic constraints on the upper mantle structure of the Hainan plume. *Phys. Earth Planet. Inter.* **2009**, *173*, 33–50. [CrossRef]

74. Huang, J. P- and S-wave tomography of the Hainan and surrounding regions: Insight into the Hainan plume. *Tectonophysics* **2014**, *633*, 176–192. [CrossRef]
75. Zhao, D. Seismic images under 60 hotspots: Search for mantle plumes. *Gondwana Res.* **2007**, *12*, 335–355. [CrossRef]